Acta Crystallographica Section A
Foundations and Advances
ISSN 2053-2733

Received 17 January 2014
Accepted 28 May 2014

Hirshfeld atom refinement for modelling strong hydrogen bonds

Magdalena Woińska,[a,b] Dylan Jayatilaka,[b] Mark A. Spackman,[b] Alison J. Edwards,[c] Paulina M. Dominiak,[a] Krzysztof Woźniak,[a] Eiji Nishibori,[d]‡ Kunihisa Sugimoto[e] and Simon Grabowsky[b]*

[a]Faculty of Chemistry, University of Warsaw, Pasteura 1, 02-093 Warsaw, Poland, [b]School of Chemistry and Biochemistry, The University of Western Australia, 35 Stirling Highway, Crawley WA 6009, Australia, [c]Australian Nuclear Science and Technology Organization, New Illawarra Road, Lucas Heights NSW 2234, Australia, [d]RIKEN RSC-Rigaku Collaboration Center, RIKEN SPring-8 Center, 1-1-1, Kouto, Sayo-cho, Sayo-gun, Hyogo 679-5148, Japan, and [e]Japan Synchrotron Radiation Research Institute (JASRI), 1-1-1, Kouto, Sayo-cho, Sayo-gun, Hyogo 679-5198, Japan. Correspondence e-mail: simon.grabowsky@uwa.edu.au

High-resolution low-temperature synchrotron X-ray diffraction data of the salt L-phenylalaninium hydrogen maleate are used to test the new automated iterative Hirshfeld atom refinement (HAR) procedure for the modelling of strong hydrogen bonds. The HAR models used present the first examples of $Z' > 1$ treatments in the framework of wavefunction-based refinement methods. L-Phenylalaninium hydrogen maleate exhibits several hydrogen bonds in its crystal structure, of which the shortest and the most challenging to model is the O—H···O intramolecular hydrogen bond present in the hydrogen maleate anion (O···O distance is about 2.41 Å). In particular, the reconstruction of the electron density in the hydrogen maleate moiety and the determination of hydrogen-atom properties [positions, bond distances and anisotropic displacement parameters (ADPs)] are the focus of the study. For comparison to the HAR results, different spherical (independent atom model, IAM) and aspherical (free multipole model, MM; transferable aspherical atom model, TAAM) X-ray refinement techniques as well as results from a low-temperature neutron-diffraction experiment are employed. Hydrogen-atom ADPs are furthermore compared to those derived from a TLS/rigid-body (*SHADE*) treatment of the X-ray structures. The reference neutron-diffraction experiment reveals a truly symmetric hydrogen bond in the hydrogen maleate anion. Only with HAR is it possible to freely refine hydrogen-atom positions and ADPs from the X-ray data, which leads to the best electron-density model and the closest agreement with the structural parameters derived from the neutron-diffraction experiment, *e.g.* the symmetric hydrogen position can be reproduced. The multipole-based refinement techniques (MM and TAAM) yield slightly asymmetric positions, whereas the IAM yields a significantly asymmetric position.

1. Introduction

Resolving positions of hydrogen atoms and an accurate description of their atomic mean displacements are significant challenges in X-ray crystallography. Since hydrogen atoms contain only one electron, density peaks in their vicinity are shifted towards their bonding partners, which makes the determination of their nuclear positions difficult. In contrast, neutrons are scattered by nuclei, which eliminates this problem. Given that neutron-diffraction measurements are associated with difficulties such as limited availability of experimental facilities, long data-acquisition times and large crystal size requirements, a popular procedure to estimate hydrogen-atom positions has been to adjust the bond lengths according to tabulated averaged X—H distances based on a set of neutron measurements (Allen *et al.*, 2006; Allen & Bruno, 2010). Recently, a different neutron-data-based method of X—H bond normalization was described (Lusi & Barbour, 2011). Likewise, hydrogen anisotropic displacement parameters (ADPs) can be estimated by comparison to similar neutron structures using a rigid-body approach (*SHADE*; Madsen, 2006). The articles by Munshi *et al.* (2008), Madsen *et*

‡ Present address: Division of Physics, Faculty of Pure and Applied Sciences, University of Tsukuba, 1-1-1 Tennodai, Tsukuba, Ibaraki 305-8571, Japan.

al. (2004) and Madsen (2012) provide good reviews of these methods. Combinations of these procedures of estimating hydrogen-atom positions and ADPs were reported even for molecules with stronger hydrogen bonds, for example for a series of 1,8-bis(dimethylamino)naphthalene salts (Hoser *et al.*, 2009; Dominiak *et al.*, 2006; Woźniak *et al.*, 2003; Mallinson *et al.*, 2003). However, in the case of particularly strong hydrogen bonds, where donor–hydrogen distances are elongated, methods based on estimating hydrogen-atom properties from averaged data may yield results far from accurate.

It is preferable to determine hydrogen-atom positions and ADPs directly from the measured data. It has been shown that the use of aspherical scattering factors taking into account the effects of covalent bonding [transferable aspherical atom models, TAAMs, such as databases of generalized pseudo-atoms (Zarychta *et al.*, 2007; Dittrich *et al.*, 2008; Volkov *et al.*, 2007; Bąk *et al.*, 2011)] leads to a much improved description of hydrogen-atom positions and thus X—H bond lengths. Depending on the database used, X—H distances generally differ by a few hundredths of an Å compared to (tabulated) bond distances derived from neutron experiments (Dittrich *et al.*, 2005, 2009; Bendeif & Jelsch, 2007; Bąk *et al.*, 2011; Dadda *et al.*, 2012). Pertaining to hydrogen-atom ADPs, there are fewer reports of successful derivation of them directly from the measured data. This has to do with the fact that in a least-squares determination the ADPs are highly correlated with parameters describing the electron density. In this context, Hirshfeld (1976) stated: '... there is no possibility of deriving hydrogen vibration parameters from the X-ray intensities'. This verdict relates to applications of the multipole model: yet, even within this model Stewart *et al.* (1975) have predicted and, *e.g.*, Zhurov *et al.* (2011) have shown that the use of polarized hydrogen atoms (taking into account an additional bond-directed dipole term) does lead to hydrogen ADPs that are in fairly good agreement with ADPs derived from neutron-diffraction data.

By contrast with the multipole model, Hirshfeld atom refinement (HAR) is a method of structural refinement in which the electron density is not refined, so that correlations between the ADPs and electron-density parameters are completely avoided. Thus, it can be expected that physically more meaningful ADPs can be derived from the refinement, especially for hydrogen atoms. Structural parameters are obtained from single-crystal X-ray diffraction data by using cycles of aspherical atom partitioning of *ab initio* quantum mechanical molecular electron densities and subsequent standard structural least-squares refinement (Jayatilaka & Dittrich, 2008). HAR combines theoretical and experimental data in the same way the independent atom model (IAM) does. This means that HAR does not use more extensive or more sophisticated theory than the IAM, but it calculates tailor-made aspherical scattering factors on the fly (instead of using tables of theoretically calculated spherical scattering factors) in order to make the most of the experimental data. Older implementations of HAR have been tested for the treatment of hydrogen atoms after a single cycle of electron-density (ED) calculation and least-squares refinement (Jayatilaka & Dittrich, 2008), and after manually alternating cycles of ED calculation and structure refinement (Dittrich *et al.*, 2012). A new implementation of HAR is now available that automatically iterates these cycles to convergence. It has been tested extensively for the accuracy and precision of determining hydrogen-atom positions, X—H distances and hydrogen-atom ADPs (Capelli *et al.*, 2014). Importantly, it has been found that HAR produces these properties in statistical agreement with the results derived from neutron-diffraction data at multiple temperatures. Therefore, the most challenging problem in this context, namely the unconstrained and unrestrained derivation of hydrogen-atom positions and ADPs for strong (symmetric) hydrogen bonds from the X-ray diffraction data, can now be tackled with this new HAR implementation.

Hydrogen maleate salts are a suitable material for hydrogen-position investigations, as they contain a strong intramolecular hydrogen bond requiring careful treatment during X-ray data processing. There are numerous studies of crystal structures of hydrogen maleate salts in the literature [a total of 88 entries in the Cambridge Structural Database (CSD)] showing that the O···O distance is constant around 2.45 Å. The O—H distances, in contrast, vary significantly and can be up to 0.4 Å shorter for highly asymmetric hydrogen bonds than for symmetric ones with a large variety of intermediate distances. Structures with a symmetric hydrogen bond in the hydrogen maleate anion occur less frequently. In some of them the symmetry of the bond is enforced by the space group used to model the crystal symmetry (hydrogen atom on a mirror plane), *e.g.* in methylammonium hydrogen maleate (Madsen *et al.*, 1998) and potassium hydrogen maleate (Wilson *et al.*, 2003) (both being neutron structures with an O—H distance of about 1.22 Å). There are also a few salts in which the observed symmetry of the hydrogen bond in the hydrogen maleate anion is not imposed by any crystallographic symmetry, such as imidazolium hydrogen maleate (Hussain *et al.*, 1980; Hsu & Schlemper, 1980) (neutron measurements), piperazinium hydrogen maleate (Jin *et al.*, 2003) and dimethylammonium hydrogen maleate (Madsen & Larsen, 1998). Such a symmetric hydrogen bond may either be an example of two shallow, almost merged energetic minima with respect to the hydrogen position, or one flat minimum, which is, according to the results of relevant studies, a common phenomenon for hydrogen maleate anions in various structures (Garcia-Viloca *et al.*, 1997; Bach *et al.*, 1997; Hodošček & Hadži, 1990; Wilson *et al.*, 2003).

A few structures with an asymmetric hydrogen site have been determined from neutron-diffraction experiments: sodium hydrogen maleate (Olovsson *et al.*, 1984), magnesium bis(hydrogen maleate) (Vanhouteghem *et al.*, 1987) and calcium hydrogen maleate (Hsu & Schlemper, 1980). However, most of the hydrogen maleate structures come from low-resolution X-ray measurements in which the position of the hydrogen atom in the intramolecular hydrogen bond is determined according to a difference-density map. This strategy may lead to very asymmetric hydrogen bonds such as 1.06/1.35 Å (James & Matsushima, 1976), 0.91/1.51 Å (Czugler

& Báthori, 2004) and 0.99/1.48 Å (Jin *et al.*, 2002). The total number of determinations deposited in the CSD with O—H bond lengths in the range 0.85–1.06 Å amounts to 34 (out of a total of 88 entries for hydrogen maleate) and, for many, the geometry of this bond may not be properly determined. Moreover, for a number of reported structures the position of the hydrogen atom in the intramolecular hydrogen bond was determined geometrically (riding model) resulting in O—H distances as short as 0.82–0.84 Å (Alagar *et al.*, 2003; Rajagopal *et al.*, 2001; Santacruz *et al.*, 2007) – in total 11 structures with a hydrogen atom positioned at this distance were found in the CSD.

Methylammonium hydrogen maleate (Madsen *et al.*, 1998) is the only electron-density study of a hydrogen maleate salt based on a refinement of high-resolution X-ray data. It was performed using atomic positions and ADPs fixed at the neutron geometry. All measurements in the literature to date were carried out at a temperature of 100 K or higher and until now, as discussed above, no attempt has been undertaken to accurately determine the position of the hydrogen atom in the hydrogen bond in the hydrogen maleate anion utilizing data from X-ray diffraction experiments. Given the huge number of crystal structures for which the description of hydrogen bonds is obviously inaccurate, the need to investigate this is clear.

The particular compound considered in this work is L-phenylalaninium hydrogen maleate. It has a crystalline structure containing various types of hydrogen bonds besides the intramolecular one of interest, and molecules form crystal networks stabilized by shorter O—H···O and longer N—H···O hydrogen bonds between the ions. The only reported prior attempt to determine the structure of L-phenylalaninium hydrogen maleate was based on low-resolution X-ray diffraction data and resulted in an asymmetric hydrogen position in the intramolecular hydrogen bond with the O—H bond lengths 1.13/1.28 Å (Alagar *et al.*, 2001). In a different X-ray study, reported for the racemic DL-phenylalaninium hydrogen maleate, all the hydrogen atoms were positioned geometrically, which led to an even more asymmetric hydrogen bond (Rajagopal *et al.*, 2001).

Here, we present the results of neutron-diffraction measurements at 12 K, which clearly indicate a fully symmetric position of the hydrogen atom, and compare with the results of a HAR of a high-resolution synchrotron X-ray diffraction measurement at 25 K. IAM, free multipole model (MM) and TAAM refinements of the same X-ray data set were carried out additionally. Both MM and TAAM are based on the Hansen–Coppens multipole model (Hansen & Coppens, 1978), but in TAAM the multipole parameters are either derived using databases of experimentally or theoretically derived generalized pseudoatoms or using tailor-made theoretical structure factors and are kept fixed during the structural refinement (Zarychta *et al.*, 2007; Dittrich *et al.*, 2008; Volkov *et al.*, 2007; Bąk *et al.*, 2011). We have chosen the latter TAAM strategy for the charged species involved here. Previous comparisons of derived properties from HAR and MM are presented in Chęcińska *et al.* (2013) and Hickstein *et al.* (2013).

Finally, we point out a novel technical aspect of this HAR study. To recapitulate, HAR uses a molecular wavefunction for deriving the aspherical scattering factors employed in the refinement. Therefore, HAR does not have basis functions at the acceptor atoms of intermolecular hydrogen bonds and might therefore introduce a systematic bias when describing hydrogen atoms involved in strong hydrogen-bonding interactions. Normally, the crystal field (including the acceptor atom) is simulated using charges and dipoles placed around the central molecule. The novel aspect in this study is that we have chosen a compound with an intramolecular hydrogen bond where both donor and acceptor atoms are described within the same wavefunction. Moreover, the two independent ions of the asymmetric unit were combined in a wavefunction calculation clustering those two to a supermolecule, so that also the second shortest hydrogen bond in the crystal structure is contained within the same wavefunction. This eliminates the discussed potential bias for those two strong hydrogen bonds.

The parameters of the two strongest hydrogen bonds are discussed in comparison to the other X-ray and neutron refinement methods using two different measures of quality of the refinements: (i) X—H bond distances and ADPs for all hydrogen atoms in the structure; and (ii) residual-density and deformation-density distributions. This allows judgment of the success of the reconstruction of the electron density in comparison to multipole-based techniques and judgment of the accuracy of the determination of hydrogen-atom properties, and it puts the findings for the strong hydrogen bonds into perspective.

2. Experimental methods

2.1. Crystallization

1 mmol of L-phenylalanine was added to a few millilitres of hot purified water. Another few millilitres were added slowly, so that all substance was dissolved upon shaking for about 30 min. Before the saturated L-phenylalanine solution cooled, one equivalent of maleic acid was added, which dissolved and reacted readily. The solution was transferred into several Petri dishes and loosely covered with glass slides. Colourless crystals of the correct size for synchrotron X-ray diffraction experiments could be harvested from the solution after several hours. In order to obtain crystals of the appropriate size for Laue neutron-diffraction experiments, the aqueous solutions were further evaporated for several days.

2.2. Neutron experiment and structure refinement

The Laue-technique neutron-diffraction experiment was carried out at the Bragg Institute of the Australian Nuclear Science and Technology Organization (ANSTO) using the instrument KOALA (Edwards, 2011) on a thermal guide at the OPAL research reactor. Laue patterns were recorded from the stationary crystal with a large cylindrical imaging-plate camera at a temperature of 12 K using a helium cryostat. Indexing, integration, normalization and reduction of data

Table 1
Experimental details.

	X-ray	Neutron
Crystal data		
Chemical formula	$C_{13}H_{15}NO_6$	
M_r	281.26	
Crystal system, space group	Monoclinic, $P2_1$	
a (Å)	10.905 (2)	
b (Å)	5.234 (1)	
c (Å)	11.439 (2)	
β (°)	101.36 (3)	
V (Å^3)	640.1 (2)	
Z	2	
Data collection		
Temperature (K)	25	12
Radiation type	Synchrotron, monochromatic	Neutron, polychromatic
Wavelength (Å)	0.354	Range: 0.850–1.700
Crystal size (mm)	0.2 × 0.1 × 0.03	1.8 × 1.6 × 0.7
Resolution d_{max} (Å)	0.45	0.60
Diffractometer	SPring-8 BL02B1, imaging-plate camera	KOALA Laue, imaging-plate camera
Extinction coefficient	—	5.6 (10)†
No. of measured, independent reflections	124185, 7820	31912, 2487
R_{int}	0.022	0.064
Completeness (%)	99.8	80.4

† Larson (1970), equation (22).

were performed *via* the program *LaueG* (Piltz, 2011), with the integration procedure being based on the Argonne boxes procedure (Wilkinson *et al.*, 1988). 31 912 reflections were measured, but only reflections with at least twofold redundancy were allowed to proceed to the data-reduction stage, so that a total of 2487 symmetry-independent reflections were finally recorded (R_{int} = 6.4%). Refinement of the structure employed the *CRYSTALS* suite of programs (Betteridge *et al.*, 2003) and commenced from atomic positions for all atoms taken from the X-ray crystal structure of the compound (see the next section). Subsequent refinement of the positional and anisotropic displacement parameters for all atoms as well as an extinction parameter led to a convergent geometry of high precision and quality. For details, see Tables 1 and 2 and the CIF (CCDC-977783) deposited with the CSD. It can be downloaded free of charge from http://www.ccdc.cam.ac.uk/Community/Requestastructure/Pages/DataRequest.aspx.

2.3. X-ray experiment and structure refinement

The X-ray diffraction experiment was carried out on the beamline BL02B1 of SPring-8, Japan. Data collection was performed at 25 K using synchrotron radiation with the wavelength of 0.354 Å. The single-crystal X-ray diffraction pattern was measured on a large cylindrical image-plate camera (Sugimoto *et al.*, 2010). Diffraction data were used up to the resolution $d \geq 0.45$ Å ($\sin\theta/\lambda \leq 1.1$ Å^{-1}) with an average completeness of 0.998. The parameters of the unit cell were determined by a least-squares fit to 20 638 strongest reflections. Integrated intensities of all Bragg reflections were obtained by the software *RAPID-AUTO* (Rigaku, 2004), which was also used for the application of Lorentz–polarization corrections. Data scaling and merging were performed with *SORTAV* (Blessing, 1987). All Friedel pairs were merged, the Flack parameter (Flack, 1983) being 0.3 (3). The experimental details and the crystallographic data are presented in Table 1.

The crystal structure was solved with *SHELXS* and the IAM refinement was performed using *SHELXL97* (Sheldrick, 2008). ADPs were refined only for non-hydrogen atoms and all the hydrogen atoms were refined isotropically during the X-ray structural refinement. This provided the starting model for the neutron-diffraction study and the subsequent X-ray refinement by three different procedures: transferable aspherical atom model, free multipole refinement according to the Hansen–Coppens formalism, and finally, substantially differing from the previous procedures, Hirshfeld atom refinement. The CIF that resides with the CSD (CCDC-977782) is based on the latter refinement procedure (subsequently referred to as HAR_shade).

2.4. Hansen–Coppens multipolar-model-based techniques

Two of the methods of electron-density refinement presented in this work, TAAM and free MM, are based on the Hansen–Coppens multipole model (Hansen & Coppens, 1978). In this formalism the electron density of a crystal is represented as a sum of pseudoatomic electron densities centred on the nuclei. The multipole refinement in each case was accomplished using the scheme implemented in the *XD2006* software (Volkov *et al.*, 2006). The refinement procedure for the TAAM and free multipole refinements was carried out on F^2 with the same constraints imposed on the parameters of the multipole model. In both cases multipole expansion up to the hexadecapolar level was used for the non-hydrogen atoms (C, N and O) with local symmetry constraints applied and coefficients κ and κ' equal for atoms of the same type. For the hydrogen atoms the multipole expansion was truncated at the quadrupolar level with only bond-directed multipoles included in the refinement (except for the most strongly hydrogen-bonded atom H1, for which all the quadrupolar multipoles were included). The X—H bond distances were constrained to averaged values obtained from neutron-diffraction data (Allen *et al.*, 2006); only the coordinates of H1 were freely refined. For chemically equivalent hydrogen atoms all the parameters of the multipole model were constrained to have equal values. The other features characteristic for TAAM and free multipole refinement are described in the two following subsections devoted individually to the two methods.

2.4.1. Transferable aspherical atom model. The TAAM is considered a substantial improvement in comparison to the IAM (Zarychta *et al.*, 2007; Dittrich *et al.*, 2008; Volkov *et al.*, 2007; Bąk *et al.*, 2011; Pichon-Pesme *et al.*, 2004) as it takes into account electron-density deformations due to bond formation or lone pairs through fixed multipole parameters. In this study, these parameters are obtained on the basis of the molecular wavefunction calculated for each of the two ions separately

Table 2
Refinement details for all the considered models.

Neutron structure; IAM; TAAM; free multipole refinement with isotropic hydrogen atoms (MM_iso) and H ADPs from *SHADE2* (MM_shade); Hirshfeld atom refinement with H ADPs refined isotropically (HAR_iso), anisotropically (HAR_aniso) or obtained by *SHADE2* (HAR_shade). GOF = goodness of fit.

	Neutron	IAM	TAAM	MM_iso	MM_shade	HAR_iso	HAR_aniso	HAR_shade
$R(F)$	0.0294	0.0291	0.0207	0.0189	0.0189	0.0200	0.0200	0.0201
$R_w(F)$	0.0290	$R_w(F^2) = 0.0703$	0.0283	0.0254	0.0253	0.0210	0.0212	0.0211
GOF	1.00	1.15	0.92	0.84	0.84	0.75	0.77	0.86
Condition for observed reflections	$F^2 > 2\sigma(F^2)$	$F^2 > 2\sigma(F^2)$	$F^2 > 2\sigma(F^2)$	$F^2 > 2\sigma(F^2)$	$F^2 > 2\sigma(F^2)$	$F > 4\sigma(F)$	$F > 4\sigma(F)$	$F > 4\sigma(F)$
No. of observed reflections	2231	7394	7394	7394	7394	7370	7370	7370
No. of parameters	317	241	199	519	504	240	315	105
$\Delta\rho_{max}$, $\Delta\rho_{min}$ (e Å^{-3})		0.47, −0.26	0.28, −0.27	0.22, −0.22	0.22, −0.21	0.21, −0.19	0.22, −0.20	0.22, −0.20

[geometry optimized in the gas phase with the *Gaussian09* program (Frisch *et al.*, 2009) using the B3LYP hybrid functional (Becke, 1993; Lee *et al.*, 1988) and the cc-pVTZ basis set (Dunning, 1989)]. As the final position of the hydrogen atom H1 upon refinement may be strongly dependent on the geometry of the anion in the wavefunction calculations, 12 different starting geometries were considered – all of them based on the IAM geometry with atom H1 shifted to slightly different positions, as described in the supporting information.[1]

The wavefunctions of the isolated anions were subsequently used to create a set of 12 different theoretical static multipole models according to the method used for construction of UBDB database entries suitable for crystallographic refinement of small organic molecules (Volkov *et al.*, 2004, 2007; Dominiak *et al.*, 2007). Complex, static structure factors based only on valence electron density for reflections with the resolution $\sin(\theta/\lambda) < 1.1$ Å^{-1} were obtained by the Fourier transform of the molecular electron densities for reciprocal-lattice points corresponding to a pseudocubic cell with 30 Å long edges (Koritsanszky *et al.*, 2002; Chandler & Spackman, 1978). The data were then processed with the *XD2006* program suite (Volkov *et al.*, 2006) – refinement of multipolar populations and contraction–expansion coefficients κ and κ' was performed according to the constraints described above.

The multipole parameters derived that way were transferred to the IAM structure. Further refinement of the overall scale factor, atomic coordinates and ADPs for non-hydrogen atoms and isotropic temperature factors for hydrogen atoms lead to 12 different TAAMs of the title compound. The figures of merit and fractal dimension plots obtained after the refinements for all 12 TAAMs can be found in the supporting information. Only one of the final 12 structures was selected for further analysis, namely the one that contains the most symmetric position of hydrogen atom H1 between oxygen atoms O1 and O2 (which is the TAAM with H1 shifted by 0.15 Å from the symmetric position in the underlying wavefunction calculation), and is hereafter referred to with the short form 'TAAM'. The details of the refinement of this TAAM structure, such as residual-density values and the other figures of merit, are collected in Table 2.

[1] Supporting information for this paper is available from the IUCr electronic archives (Reference: KX5029).

2.4.2. Free multipole refinement. The free refinement was started with the structure from one of the TAAMs. No charge transfer between the anion and the cation was allowed. Additional symmetry constraints for the atom O6 (*mm*2 symmetry) had to be imposed in order to improve deformation-density maps. First, multipole moments up to hexadecapoles were gradually included in the refinement. In the next stage, atomic positions, isotropic hydrogen-atom and anisotropic non-hydrogen-atom displacement parameters were additionally refined. Subsequently only κ parameters for non-hydrogen atoms were refined, and finally all the specified parameters together. In several final cycles of refinement, κ values were kept fixed. The model obtained at this stage of refinement, with isotropically refined hydrogen atoms, is further referred to as MM_iso. Afterwards, ADPs of hydrogen atoms were estimated using the *SHADE2* server (Madsen, 2006), as their free refinement was not feasible. The described refinement scheme was repeated until convergence was reached of estimated hydrogen ADPs. The geometry of the structure is reported at this stage of the refinement using the name MM_shade. The details for MM_iso and MM_shade refinements are listed in Table 2.

As in the case of the TAAM refinement, for both MM_iso and MM_shade all the X—H distances (except those in the intramolecular hydrogen bond O1—H1···O2) were fixed at the averaged values estimated from neutron-diffraction data. Constraints were also required on the quite short O5—H5···O3 hydrogen bond. Additional tests proved that removing the constraints applied to the O5—H5 distance gave a physically incorrect description of this bond with the bond length reduced to 0.943 Å. A similar conclusion can be drawn in the case of the TAAM refinement.

2.5. Hirshfeld atom refinement

HAR (Jayatilaka & Dittrich, 2008; Capelli *et al.*, 2014), as opposed to the previous methods, does not invoke the concept of the multipolar model, but introduces Hirshfeld stockholder partitioning (Hirshfeld, 1977) of an *ab initio* calculated molecular electron density for generating aspherical scattering factors used in the geometry refinement. Specifically, the density of an atom in the Hirshfeld partition $\rho_A(\mathbf{r})$ at a given point of space is the total electron density of the molecule $\rho(\mathbf{r})$ scaled by the appropriate atomic weight function $w_A(\mathbf{r})$:

$$\rho_A(\mathbf{r}) = w_A(\mathbf{r})\rho(\mathbf{r}), \quad w_A(\mathbf{r}) = \frac{\rho_A^0(\mathbf{r}-\mathbf{R}_A)}{\sum_B^{\text{molecule}} \rho_B^0(\mathbf{r}-\mathbf{R}_B)}. \quad (1)$$

The weight function of the atom A is given as a ratio of the spherically averaged atomic electron density of this atom $\rho_A^0(\mathbf{r}-\mathbf{R}_A)$ (with $\mathbf{R}_A$ being the position of the nucleus) to the density of a promolecule constructed of the spherically averaged atomic densities of all the component atoms. The convolution of the Hirshfeld atomic density ρ_A with the probability distribution function for the nucleus A leads to the thermally averaged density $\overline{\rho}_A$, which, subjected to Fourier transform, gives the thermally averaged aspherical Hirshfeld atomic scattering factor $\overline{f}_A$. Next, $\overline{f}_A$ is used in HAR for calculating model structure-factor magnitudes according to the following expression:

$$F_{\text{calc}}(\mathbf{k}) = \left| \sum_{(\mathbf{S},\mathbf{t})}^{\text{symops}} \exp(i\mathbf{k}\mathbf{t}) \sum_A^{\text{atoms}} n_A^{-1} \exp(i\mathbf{k}\mathbf{R}_A)\overline{f}_A(\mathbf{S}^T\mathbf{k}) \right|. \quad (2)$$

In the above equation $\mathbf{k}$ is a scattering vector labelling a reflection, the first sum runs over a set of crystal space-group symmetry operations ($\mathbf{S}$, rotation matrix; $\mathbf{t}$, translation vector), and the second sum runs over the atoms in an asymmetric unit (with n_A being a site-symmetry factor of atom A at the position R_A). The procedure is implemented in the *TONTO* program (Jayatilaka & Grimwood, 2003). HAR, compared to the multipole model, allows more flexibility in selecting the quantum-mechanical method and basis set adjusted for a particular problem; furthermore, local coordinates do not need to be specified, and block release of parameters is never performed. On the other hand, *ab initio* calculations of wavefunctions make the refinement much more computationally demanding. To simulate the wavefunction of a molecule in a crystalline medium more accurately, the wavefunction may be calculated for a molecule surrounded with clusters of point charges and dipoles (imitated by two opposite charges separated by a short distance) located at the atomic sites. After obtaining the molecular wavefunction, cluster charges and dipoles are updated and the procedure is repeated until convergence.

In previous versions of HAR (Jayatilaka & Dittrich, 2008) a 'rigid atom approximation' was used, whereby the Hirshfeld atoms were determined once and were then held fixed during the refinement procedure. It became clear that this approximation had to be released, so that in later applications (Dittrich *et al.*, 2012) scattering-factor determination (called an 'ED step') and structural refinement steps were manually iterated. Very recently, this iteration of ED steps and refinement steps has been automated and convergence criteria were tested and implemented (parameter shifts divided by the standard uncertainties of the parameters must be less than 0.01) (Capelli *et al.*, 2014). The present study deals with the validation of the new iterative HAR procedure using the case of strong hydrogen bonds; further details about the new procedure can be found in Capelli *et al.* (2014).

HAR of L-phenylalaninium hydrogen maleate was carried out starting with the geometry from the IAM refinement. Cluster charges and dipoles used in the *ab initio* calculations were included on all atoms on all surrounding molecules having at least one atom within the radius of 8 Å. The molecular wavefunction was calculated using the DFT method (Hohenberg & Kohn, 1964) with the BLYP functional (Becke, 1993; Lee *et al.*, 1988) and the cc-pVTZ basis set (Dunning, 1989). The refinement was performed on F and only the reflections with $F > 4\sigma(F)$ were taken into account. The refined parameters were atomic positions and ADPs for all atoms including H atoms (the name of the resulting structure: HAR_aniso). The scale factor is optimized but not included in the least-squares; however, this may affect only estimated standard deviations of the obtained parameters. Although ADPs for hydrogen atoms could be refined to convergence (unlike in the case of the multipole model), the shapes of some ellipsoids were elongated and their orientations oblique. Therefore, the values of the hydrogen ADPs were additionally calculated using the *SHADE2* server (Madsen, 2006) and fixed in a new HAR calculation in order to allow comparison with a different model with trusted hydrogen-atom ADPs (HAR_shade). For the sake of completeness and comparison with the free multipole refinement, the results of HAR with isotropically refined hydrogen atoms (HAR_iso) are also included in further analysis.

At present, the HAR algorithm used in the *TONTO* program is optimized and tested only for refining structures with at most one molecule per asymmetric unit. More than one molecule can be treated by considering the asymmetric unit as a 'supermolecule' composed of several individuals. This requires a suitable choice of a symmetric cluster model to avoid systematic errors, which in turn makes the choice of the asymmetric unit crucial. The procedure can be accurate if there is a strong intermolecular interaction between the considered molecules inside the asymmetric unit, such as hydrogen bond O5—H5···O3 in this study. Some problems within the HAR models, such as highly stretched hydrogen ADPs, may be ascribed to the $Z' > 1$ treatment; although they could also simply result from insufficient experimental information. More investigation is necessary, and alternative procedures of refining structures with more than one molecule in an asymmetric unit will be published as a separate study.

3. Results

3.1. Quality of the refinement

3.1.1. Figures of merit, *X*—H distances and ADPs. The figures of merit obtained in the refinement of the structures performed according to all the described methods are listed in Table 2. The values of the statistical parameters $R(F)$ (amounting to 2% for HAR, insignificantly higher for TAAM and slightly lower for MM) and $R_w(F)$ (approximately 2.8% for TAAM, 2.5% for MM and 2.1% for HAR) are low and quite similar for all the cases. This confirms the good quality of the crystal data and the correctness of the fitting models of electron density. The maximal and minimal values of residual

Table 3
The X—H distances for selected hydrogen atoms (in Å) resulting from various refinement methods.

The TAAM/MM distances are standard averaged values derived from neutron measurements.

Method	C2—H2 hydrogen maleate ring	N1—H41 ammonium group	C6—H6 methine group	C7—H71 methylene group	C11—H11 phenyl group
IAM	0.931 (11)	0.860 (12)	0.990 (8)	1.024 (12)	0.991 (11)
Neutron	1.087 (2)	1.038 (2)	1.092 (2)	1.096 (3)	1.088 (3)
TAAM/MM	1.083	1.036	1.098	1.092	1.083
HAR_iso	1.065 (11)	1.024 (14)	1.102 (9)	1.086 (10)	1.098 (11)
HAR_aniso	1.050 (10)	1.037 (13)	1.100 (10)	1.075 (10)	1.099 (10)
HAR_shade	1.066 (10)	1.022 (10)	1.101 (9)	1.089 (10)	1.096 (10)

density are reasonably low and very similar for all the HAR and MM structures (residual densities within the range ± 0.22 e Å^{-3}) and for the TAAM they are marginally higher ($\Delta\rho_{\min} = -0.28$ e Å^{-3} and $\Delta\rho_{\max} = 0.29$ e Å^{-3}).

The quality of the performed refinements can be further assessed *via* comparison of the X—H bond lengths estimated on the basis of X-ray data to those obtained for the neutron structure. In this section we consider only the X—H distances not involved in the intramolecular (O1—H1···O2) and the shortest intermolecular (O5—H5···O3) hydrogen bond (the two latter hydrogen bonds are the subject of a detailed analysis presented in §3.2, where the parameters of all the remaining hydrogen bonds are also briefly discussed). Selected X—H distances for hydrogen atoms representative of certain types of functional groups are reported in Table 3; the remaining X—H distances are given in the supporting information.

The average neutron distances applied in the case of the multipole-model-based refinements (MM/TAAM) are in best agreement with the present neutron experiment as expected. As far as HAR is concerned, the freely refined X—H distances are in remarkable agreement with the results from neutron diffraction. The different kinds of X—H bonds from different functional groups are differentiated, *i.e.* the subtle geometry differences are reflected in the HAR results. However, the differences between the obtained bond lengths and the neutron measurement vary without any specific trend for different kinds of X—H bonds, with variance less than 0.05 Å. It is difficult to discern any particular differences in the quality of X—H distance estimation among the three HAR models.

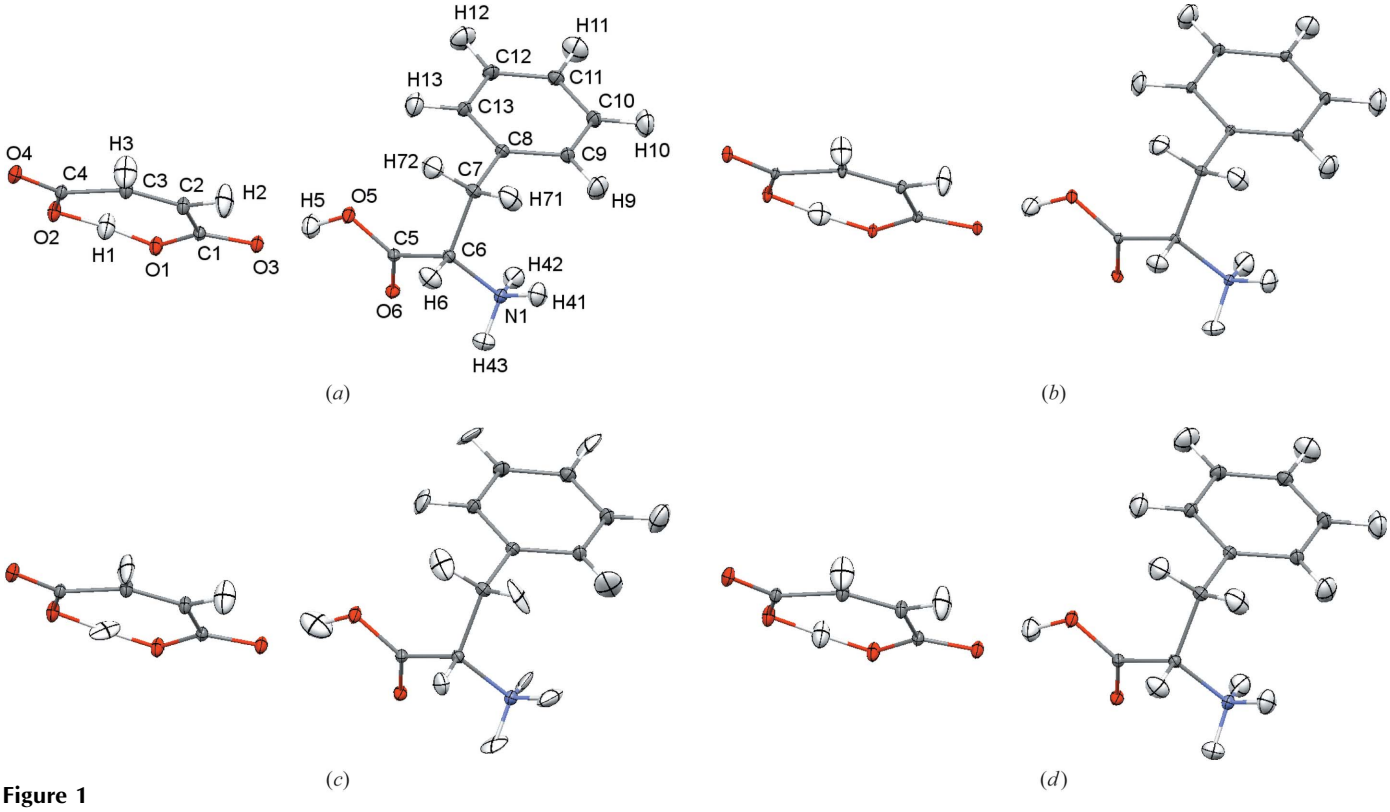

Figure 1
Structure and ADPs of L-phenylalaninium hydrogen maleate obtained for various refinement strategies: (*a*) MM_shade (free multipole refinement, H ADPs from *SHADE2*), (*b*) neutron-diffraction study (all ADPs refined), (*c*) HAR_aniso (Hirshfeld atom refinement, all the ADPs refined), (*d*) HAR_shade (Hirshfeld atom refinement, H ADPs from *SHADE2*). The picture presents the geometry of the asymmetric unit. The ellipsoids are depicted at the 50% probability level.

Table 4
The values of ADPs (in Å^2) of selected hydrogen atoms for various refinement strategies (neutron, HAR_aniso, HAR_shade and MM_shade).

The ADPs are expressed in the crystal coordinate system. Averaging statistics of the comparisons between the ADPs from different models (neutron, HAR_aniso, HAR_shade) refer to the full set of atoms. Mean absolute difference (MAD) $\langle|\Delta U_{ij}|\rangle$ with its mean standard deviation σ_{mean} (both in Å^2); mean difference (MD) $\langle\Delta U_{ij}\rangle$ with corresponding σ_{mean} (both in Å^2); wRMSD = root-mean-square difference weighted by the combined standard uncertainty (csu) $[\langle(\Delta U_{ij}/\text{csu})^2\rangle]^{1/2}$ with csu(X-ray, neutron) = [su(X-ray)^2 + su(neutron)^2]$^{1/2}$; mean ratio (MR) $\langle r\rangle = \langle U_{ii}(\text{X-ray})/U_{ii}(\text{neutron})\rangle$ for the diagonal elements. The mean standard deviations given here are used to express the error in the mean; they are not the population standard deviations used in similar studies, compare *e.g.* Morgenroth *et al.* (2008), Capelli *et al.* (2014). The experimental errors given in parentheses in the first part of the table are the least-squares standard uncertainties (su's) used to calculate the csu's. See further discussion of these statistical properties in Schwarzenbach *et al.* (1995).

	Model	U_{11}	U_{22}	U_{33}	U_{12}	U_{13}	U_{23}
H1	Neutron	0.0220 (10)	0.0150 (8)	0.0229 (10)	−0.0033 (7)	0.0043 (9)	−0.0007 (7)
	HAR_aniso	0.0226 (54)	0.0095 (51)	0.0530 (120)	−0.0088 (42)	0.0151 (62)	−0.0064 (61)
	HAR_shade	0.0323	0.0216	0.0142	−0.0046	0.0074	−0.0029
	MM_shade	0.0328	0.0218	0.0154	−0.0043	0.0083	−0.0032
H2	Neutron	0.0375 (14)	0.0145 (8)	0.0142 (8)	−0.0080 (9)	0.0070 (9)	−0.0063 (7)
	HAR_aniso	0.0473 (52)	0.0226 (48)	0.0164 (41)	−0.0100 (41)	0.0107 (38)	−0.0022 (36)
	HAR_shade	0.0503	0.0206	0.0205	−0.0121	0.0077	−0.0084
	MM_shade	0.0503	0.0209	0.0208	−0.0109	0.0079	−0.0084
H41	Neutron	0.0233 (11)	0.0191 (9)	0.0201 (9)	−0.0018 (8)	0.0058 (9)	−0.0107 (8)
	HAR_aniso	0.0229 (43)	0.0352 (63)	0.0352 (61)	−0.0095 (44)	0.0167 (41)	−0.0155 (54)
	HAR_shade	0.0259	0.0219	0.0228	0.0007	0.0045	−0.0111
	MM_shade	0.0260	0.0219	0.0237	0.0000	0.0043	−0.0109
H5	Neutron	0.0199 (9)	0.0188 (9)	0.0185 (9)	−0.0025 (8)	0.0081 (8)	−0.0045 (8)
	HAR_aniso	0.0277 (61)	0.0261 (72)	0.0408 (76)	−0.0074 (58)	−0.0044 (53)	0.0085 (63)
	HAR_shade	0.0265	0.0259	0.0187	−0.0055	0.0066	−0.0084
	MM_shade	0.0269	0.0259	0.0193	−0.0060	0.0066	−0.0081
H6	Neutron	0.0146 (8)	0.0139 (8)	0.0180 (9)	0.0039 (6)	0.0009 (8)	0.0035 (7)
	HAR_aniso	0.0197 (34)	0.0298 (50)	0.0074 (32)	0.0009 (35)	0.0048 (27)	0.0045 (33)
	HAR_shade	0.0199	0.0188	0.0232	0.0029	−0.0011	0.0032
	MM_shade	0.0212	0.0191	0.0231	0.0019	−0.0010	0.0038
H71	Neutron	0.0206 (10)	0.0124 (8)	0.0248 (10)	0.0006 (7)	−0.0002 (9)	−0.0037 (8)
	HAR_aniso	0.0401 (58)	0.0143 (42)	0.0343 (49)	0.0011 (44)	−0.0174 (42)	−0.0091 (39)
	HAR_shade	0.0255	0.0183	0.0328	0.0011	−0.0018	−0.0081
	MM_shade	0.0256	0.0195	0.0328	0.0010	−0.0016	−0.0086
H11	Neutron	0.0253 (11)	0.0282 (11)	0.0206 (10)	0.0140 (10)	0.0021 (9)	0.0055 (9)
	HAR_aniso	0.0303 (41)	0.0290 (53)	0.0227 (49)	0.0103 (39)	0.0168 (36)	0.0119 (42)
	HAR_shade	0.0294	0.0329	0.0263	0.0133	−0.0010	0.0074
	MM_shade	0.0305	0.0325	0.0274	0.0134	−0.0007	0.0072

Comparison	$\langle\lvert\Delta U_{ij}\rvert\rangle$	σ_{mean}	$\langle\Delta U_{ij}\rangle$	σ_{mean}	wRMSD	$\langle r\rangle$
HAR_aniso–neutron	0.0081	0.0006	0.0042	0.0009	1.89	1.40
HAR_aniso–HAR_shade	0.0080	0.0008	0.0030	0.0010	N/A	1.23
HAR_shade–neutron	0.0033	0.0003	0.0012	0.0005	N/A	1.20

The distances resulting from IAM are in turn significantly too short and this method clearly fails.

The evaluation of the ADPs of the structures resulting from MM_shade, HAR_aniso and HAR_shade and comparison to the neutron study is another test of the quality of the refinement methods (see Fig. 1). In all three cases of X-ray refinement the ellipsoids of non-hydrogen atoms drawn at the 50% probability level have bigger volumes than those resulting from the neutron-diffraction experiment (temperature difference of 13 K). This difference in size is not conspicuous for the hydrogen ADPs, so that for them comparison of the individual values and averaged differences quantitatively expressed in statistical properties is meaningful (Table 4).

Hydrogen ADPs determined with *SHADE2* are naturally very similar for both structures MM_shade and HAR_shade and resemble the ADPs of the neutron structure in terms of size and orientation very closely (Fig. 1). The mean absolute difference (MAD) between the hydrogen ADPs derived from HAR_shade and the neutron data is ∼0.003 Å^2 (Table 4). The signed mean difference (MD) as well as the mean ratio (MR) show that the sizes of the hydrogen ADPs estimated by *SHADE2* are bigger on average than for the neutron structures, which could simply be the temperature effect observed for the non-hydrogen ADPs. But there are also slight differences in the directions of the principal axes. The ellipsoid of the H5 atom determined by *SHADE2* in each case is a little tilted relative to the axis of the almost linear O5—H5···O3 bond – an effect not observed for the neutron structure (Fig. 1). In the case of H1, in turn, the shape of the ellipsoid obtained for the neutron structure is more spherical than for MM_shade and HAR_shade with a small inclination of the main ellipses (relative to the axis of the intramolecular hydrogen bond O1—H1···O2) that is not present in MM_shade and HAR_shade.

More variable ADPs are obtained from HAR (Fig. 1 and Table 4). In the structure HAR_aniso, practically all of the H ellipsoids are more oblate than in MM_shade, HAR_shade and the neutron structure, and many of them are also oblique. These effects are striking in the case of the atom H1, for which the ellipsoid is, on account of the very strong and symmetric hydrogen bond, expected to be rather symmetrically shaped and not inclined towards any of the O atoms. Moreover, the

ADPs obtained in the HAR procedure are determined with much lower precision than those from the neutron-diffraction experiment (by roughly a factor of five, Table 4). The ellipsoids in the structure HAR_aniso which are oblate are characterized by one (less often two) diagonal term noticeably higher than for the remaining methods (compare H1, H41, H5 and H71). For the more oblique ellipsoids, in turn, one of the off-diagonal components is significantly bigger (H1, H41, H71 and H11). The large standard uncertainties indicate that there is limited information in the X-ray data for determination of the hydrogen ADPs or a problem with the *ab initio* model itself. Perhaps the wavefunction chosen is not ideal for refinement of structures with more than one molecule per asymmetric unit.

Despite the discussed problems with the ADPs, the X—H bond lengths resulting from HAR_aniso are the most reliable compared to the structure from the neutron-diffraction experiment (see Table 3 in this subsection and the results presented in §3.2 in Tables 6 and 7). In order to resolve this apparent contradiction, a closer look at the statistical quantification of the differences of the hydrogen ADPs from HAR_aniso compared to those derived from *SHADE2* and the neutron experiment is necessary (Table 4). The mean absolute differences are ∼0.008 Å^2 each, which is less than three times larger than the difference between *SHADE2* and the neutron experiment, and about a third to a fifth of the individual diagonal ADP values. The MD and MR values are not significantly bigger than for the comparison *SHADE2*–neutron. The HAR_aniso–neutron difference is within less than two combined standard uncertainties (wRMSD), which is a remarkably close agreement given the problems from the visual inspection of the plots in Fig. 1. Overall this is the same order of magnitude of agreement found for the compound glycyl-L-alanine studied in Capelli *et al.* (2014), where the agreement between HAR- and neutron-derived hydrogen ADPs is very good. This means that – within the low precision of the determination in HAR – the hydrogen ADPs do not differ unreasonably from the values determined in the neutron-diffraction experiment, so that the oblateness and obliqueness of the hydrogen ADPs found in Fig. 1 do not express unacceptable statistical inaccuracy. Therefore, the model HAR_aniso should not be disregarded, but the good agreement in X—H bond distances is likely not to be a coincidence.

Since all the figures of merit, as well as residual- and deformation-density maps, are very similar for MM_iso and MM_shade structures, representative results for the structure MM_shade are included. Likewise, based on the discussion in the preceding paragraph, only the HAR_aniso structure is analysed in the next subsections. The maps of deformation and residual density for the structures MM_iso, HAR_iso and HAR_shade are available in the supporting information.

3.1.2. Comparison of residual- and deformation-density maps. In this section the residual density and deformation density of the three selected electron-density models are analysed in order to give an insight into the differences in the modelling of the structure, especially of the intramolecular hydrogen bond O1—H1···O2 and the strongest intermolecular hydrogen bond O5—H5···O3. The residual- and deformation-density maps are presented only in the plane of the ring of the hydrogen maleate anion. Corresponding maps in planes of other regions of both anion and cation are in agreement with all the conclusions concerning the discussed density models and can be found in the supporting information.

The minimum and maximum values of residual density for the crystal of L-phenylalaninium hydrogen maleate are already quite low for the IAM structure (see Table 2), with $\Delta\rho_{\min}$ comparable with the TAAM structure. These values are even lower for the structures MM_shade and HAR_aniso. The described differences are also confirmed by the fractal analysis of residual density, which was performed in the entire unit cell using the program *jnk2RDA* (Meindl & Henn, 2008). The fractal dimension plots (Fig. 2) show the logarithm of the

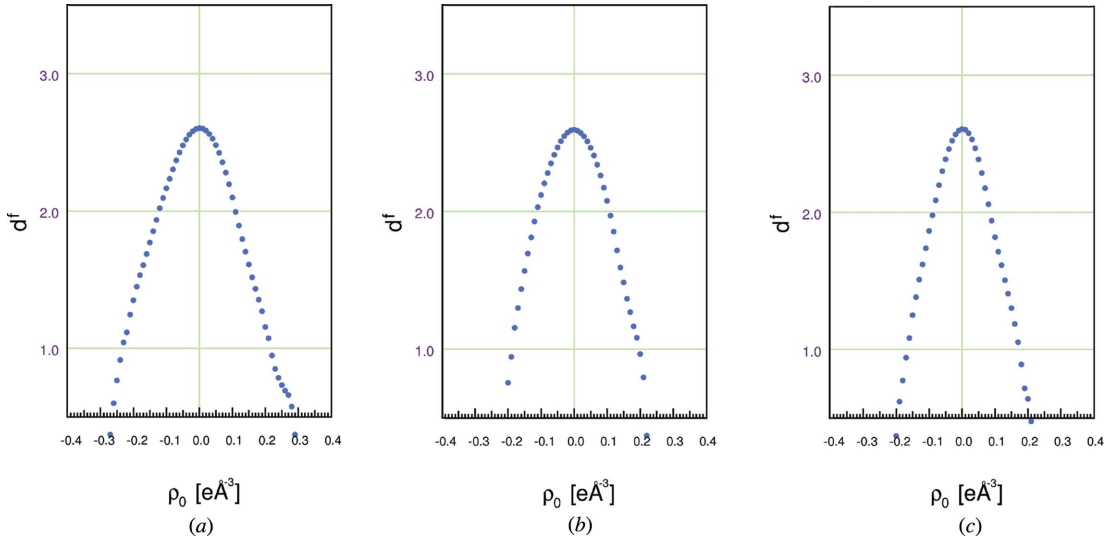

Figure 2
Fractal dimension plots (fractal dimension d^f *versus* residual density ρ_0) obtained after different refinement procedures: (*a*) TAAM, (*b*) MM_shade, (*c*) HAR_aniso.

distribution of residual densities as a function of the residual density itself after dimensional rescaling. All the presented plots are fairly symmetric and close to the parabolic distribution which would be obtained for the ideal case of residual density characterized by purely Gaussian noise. The graphs are also thin, which indicates that the deviation of the model from the data is small. However, the TAAM and MM models give rise to a small discernible shoulder on the right flank, which agrees with a minor systematic effect in the residual-density maps of Figs. 3(*a*) and 3(*b*) (contour level 0.05 e Å^{-3}), where the otherwise small residual density is arranged in alternating stripes of prevailing negative and positive values, aligned in a certain direction, similar to the direction of the crystallographic axis 2_1. The areas of nonzero residual density are remarkably smaller for HAR_aniso than for the two other models (Fig. 3*c*), which agrees with the fact that the graph in Fig. 2(*c*) is nearly perfectly symmetric, and also about a third

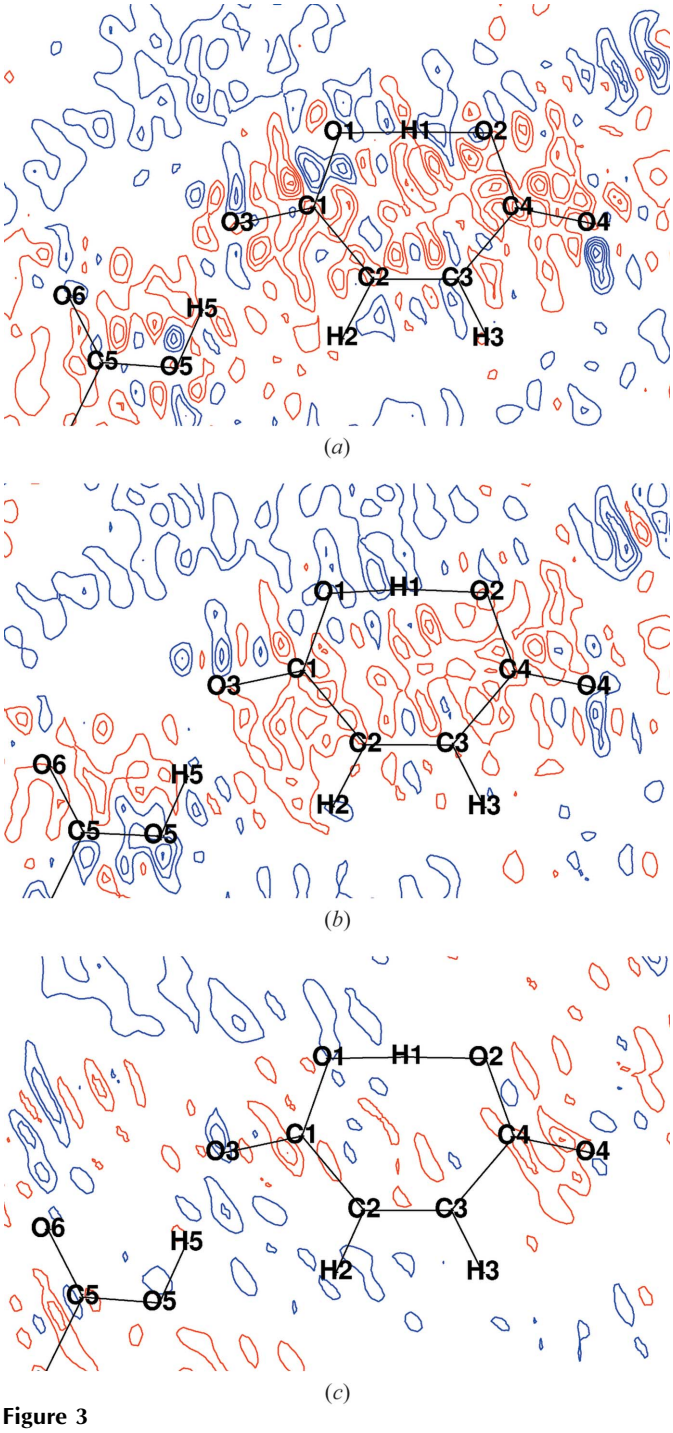

Figure 3
Residual-density maps in the plane of the ring for the hydrogen maleate anion obtained after different refinement procedures: (*a*) TAAM, (*b*) MM_shade, (*c*) HAR_aniso. Contour level 0.05 e Å^{-3}, blue – positive, red – negative.

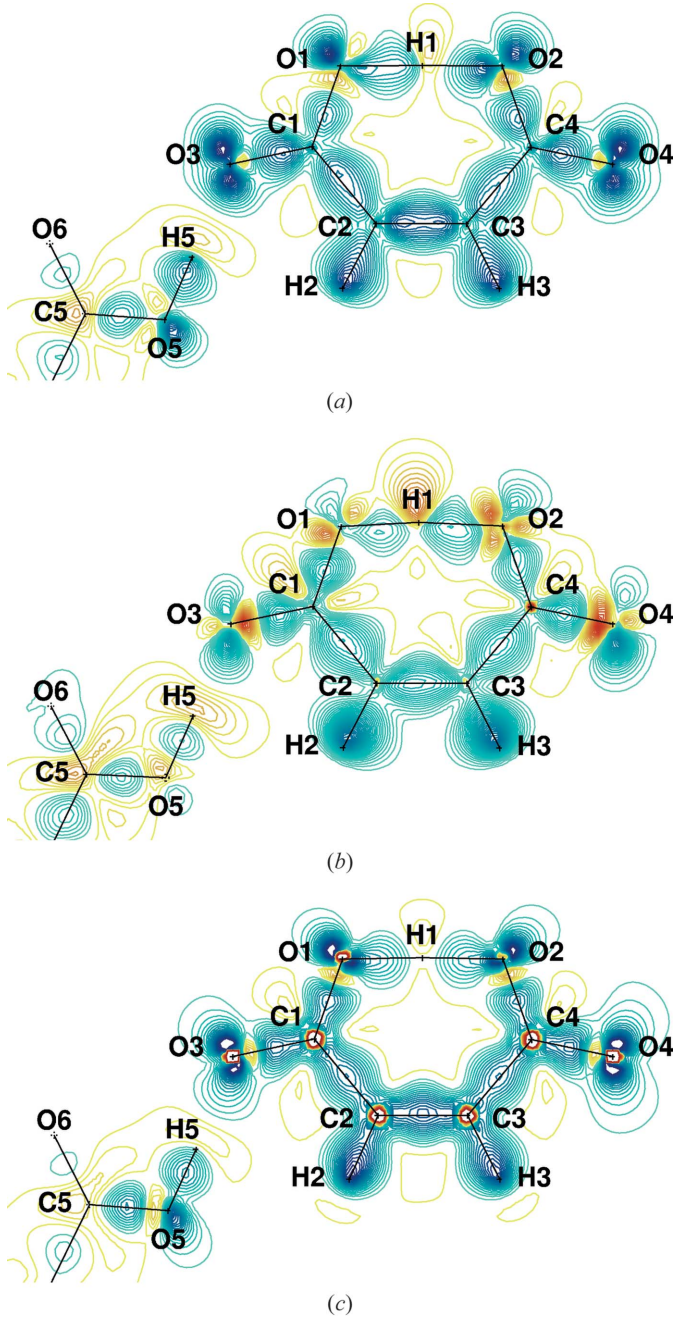

Figure 4
Deformation-density maps in the plane of the ring for the hydrogen maleate anion obtained after different refinement procedures: (*a*) TAAM, (*b*) MM_shade, (*c*) HAR_aniso. Contour level 0.05 e Å^{-3}; blue – positive; red, yellow – negative.

thinner than the one for the TAAM. HAR_aniso has strikingly few regions of residual density beyond the values of ± 0.1 e Å^{-3}, which is an excellent basis for any chemical interpretation of the corresponding electron-density parameters and structural properties. For all the structures no meaningful residual density is found in the region of the atom H1, which is again particularly clear for the structure HAR_aniso having no residual density around H1 at the given contour interval.

Deformation-density maps show electron density concentrated in the bonding and lone-pair regions. The maps (Fig. 4) reveal certain differences between the considered models and are a helpful tool in the evaluation of the density distribution. The superiority of deformation density obtained as a result of HAR compared to the two other methods is evident: the regions of positive deformation density for the HAR_aniso structure have a smooth shape and the lone pairs for all the oxygen atoms are clearly visible. The other feature showing the superiority of HAR is the presence of circular regions of negative deformation density around the nuclei of the non-hydrogen atoms, a characteristic that is not observed for the multipole-based models. This deficiency of the standard multipole model has been noted before and there are efforts to improve the description of the core regions by expanding the standard multipole model (Zhurov & Pinkerton, 2013; Fischer *et al.*, 2011; Bindzus *et al.*, 2014). In the case of HAR_aniso, deformation density in the region of the hydrogen maleate ring is the most symmetric, which is particularly clear for the intramolecular hydrogen bond and allows evaluation of the influence of the intermolecular interactions on the density and structure of the anion.

The deformation density of the hydrogen maleate ring for the TAAM structure is more asymmetric in the region of the O1—H1···O2 hydrogen bond than in the other models. Electron pairs of the oxygen atoms O1 and O2 bonding atom H1 are distributed less symmetrically around the bonds, which is particularly pronounced for O1. This type of asymmetry is even more striking for the MM_shade model. Moreover, the

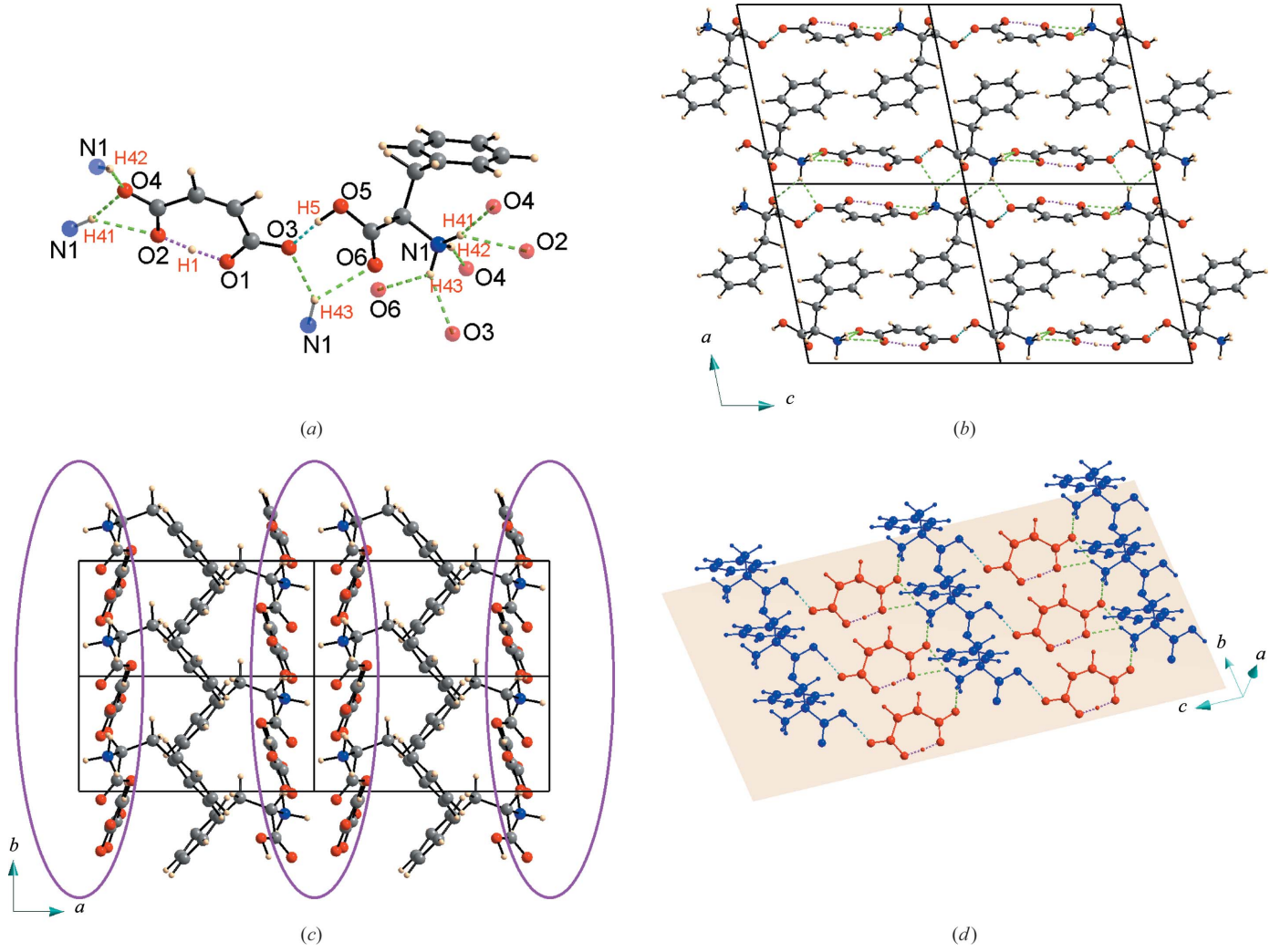

Figure 5
Crystal packing and hydrogen-bond motifs in the L-phenylalaninium hydrogen maleate crystalline structure: (*a*) hydrogen bonds in the asymmetric unit, (*b*) *b*-axis projection, (*c*) *c*-axis projection (hydrophilic layers highlighted with violet lines), (*d*) single layer – chequered pattern (anions – red, cations – blue). Hydrogen bonds marked with coloured dashed lines. Colour coding of hydrogen bonds: intramolecular – magenta, strongest intermolecular – cyan, other – green.

Table 5
Geometry of hydrogen bonds derived from the neutron-diffraction experiment (units of distances and angles: Å, °).

Bond	D—H	H···A	D···A	D—H···A
O1—H1···O2^{i}	1.209 (3)	1.208 (3)	2.4163 (17)	176.0 (3)
O5—H5···O3^{i}	1.053 (3)	1.475 (3)	2.5231 (21)	173.3 (3)
N1—H41···O4^{ii}	1.038 (3)	1.952 (3)	2.9723 (19)	166.9 (3)
N1—H41···O2^{ii}	1.038 (3)	2.218 (3)	2.9763 (15)	128.4 (2)
N1—H42···O4^{iii}	1.041 (3)	1.976 (3)	2.9803 (19)	161.2 (3)
N1—H43···O3^{iv}	1.032 (2)	2.100 (3)	2.9978 (15)	144.0 (2)
N1—H43···O6^{iv}	1.032 (2)	2.276 (3)	2.9753 (15)	123.7 (2)

Symmetry codes: (i) x, y, z; (ii) $x, y+1, z+1$; (iii) $x, y, z+1$; (iv) $-x, y+\frac{1}{2}, -z$.

deformation density of lone electron pairs of O atoms in the hydrogen maleate anion is weakly pronounced, particularly for O1 and O4. The other effect observed for this structure is the shift of positive deformation density towards the region of the ring opposite the hydrogen bond (especially around H2 and H3), leaving quite large areas of negative deformation density around the atoms O1, O2 and H1 (possibly a consequence of eliminating charge transfer between the anions in the refinement procedure).

A conclusion valid for all the models is that intermolecular interactions such as the strong O5—H5···O3 bond and the other intermolecular hydrogen bonds (not shown in the pictures, but described in §3.2) seem not to distort the electron density of the anion. The fact that these H-atom bonds do not generate a significantly asymmetric environment for the anion might be the reason for the high symmetry of the intramolecular hydrogen bond (see the next section).

We note that the agreement of the model electron density with the measured diffraction pattern is higher in a purely theoretical calculation based on an experimental geometry (HAR) than after experimentally refining parameters of an electron-density model (MM). In fact, HAR surpasses both multipole-based methods (MM and TAAM) with regard to all criteria described in this section. This is most likely due to the choice of a sufficiently high level of theory in the HAR refinement with a flexible basis set, in contrast to the inflexible radial functions used in the standard multipole model. The effect of an X-ray constrained wavefunction fitting subsequent to HAR will be discussed elsewhere.

3.2. Crystal packing and hydrogen-bond analysis

The crystal structure of L-phenylalaninium hydrogen maleate is formed by alternating hydrophilic and hydrophobic layers with alignment parallel to the (100) crystallographic plane (Fig. 5). Each hydrophilic layer consists of two hydrogen maleate columns related by 2_1 symmetry interacting with polar groups of the protonated amino acid. Within a single layer, the anions and amino-acid groups are arranged in a chequered pattern, in which they are held together by a hydrogen-bonding network (Fig. 5*a*) constituted by two hydrogen bonds between the ammonium group and the oxygen atoms of the first anion (N1—H41···O4 and N1—H42···O2), one hydrogen bond between the ammonium group and the oxygen atom of the second anion (N1—H42···O4), and the strongest intermolecular hydrogen bond observed between the carboxyl group of the amino acid and the oxygen atom of a third anion on the opposite side (O5—H5···O3). A single slab and the hydrogen bonds existing within it are illustrated in Fig. 5(*d*). These planar architectures are linked in pairs by a network of hydrogen bonds between ammonium groups and carbonyl oxygen atoms (N1—H43···O6 and N1—H43···O3) to create a hydrophilic layer (Fig. 5*b*). All the intermolecular hydrogen bonds are relatively strong (for the parameters obtained in the neutron experiment see Table 5, for the illustration see Fig. 5*a*); however, the strongest of them is evidently the O5—H5···O3 bond between the carboxyl group of the amino acid and one of the carbonyl O atoms of the anion. Hydrophobic layers are in turn built of L-phenylalaninium side chains, with mutual interdigitation by phenyl rings alternately belonging to the top and the bottom layer of the amino-acid cations (Figs. 5*b* and 5*c*). The neighbouring chains are related by 2_1 symmetry with the dihedral angle between the planes of the phenyl rings being equal to 80.94 (9)° (value from the neutron-diffraction experiment). The number of interactions observed within the hydrophobic layers is much smaller than for the hydrophilic ones; however, the crystal structure is also stabilized by short contacts existing between some hydrogen atoms from the phenyl ring and adjacent aromatic rings or atoms belonging to the hydrogen maleate anions.

The strongest of all the hydrogen bonds present in the L-phenylalaninium hydrogen maleate crystal is unquestionably the intramolecular hydrogen bond O1—H1···O2. This can be seen in Table 6, which presents the bond lengths and angles obtained in the course of six different strategies of X-ray data refinement based on aspherical scattering factors, juxtaposed with the parameters resulting from the refinement of the neutron data and the IAM structure. In each of the eight discussed cases the ring of the hydrogen maleate anion is not entirely flat, since the bonds formed by O1 and O2 appear to be slightly twisted and these two atoms are displaced a little in opposite directions with respect to the plane in which all the other atoms constituting the ring remain. For the structures obtained in a free multipole refinement (MM_iso and MM_shade) and the IAM model, O2 is also in the plane of the ring and O1 is slightly more displaced. For all the structures the torsion angle C1—C2—C3—C4 is about 2° (Table 6), which quantifies the twist.

The intramolecular hydrogen bond in the hydrogen maleate anion is symmetric according to the neutron measurement, with O1—H1/O2—H1 distances amounting to 1.209 (3)/1.208 (3) Å. Hence, one can conclude that the environment of interactions of the anion in the considered structure is quite symmetric, *i.e.* the influence of the intermolecular hydrogen bonds involving O2 and O4 (N1—H42···O4, N1—H41···O4 and N1—H41···O2) is counterbalanced by the hydrogen bonds including the atom O3 on the opposite side of the anion (O5—H5···O3 and N1—H43···O3). The bonds linking H1 with O1 and O2 are tilted insignificantly outwards from the ring [the angle O1—H1—O2 is equal to 176.0 (3)°]. The same effect and a very similar angle is observed for TAAM,

Table 6
Geometry of the intramolecular hydrogen bond O1—H1···O2 and selected torsion angles for the hydrogen maleate anion obtained with various refinement methods (units of distances and angles: Å, °).

Model	O1—H1	H1···O2	O1···O2	O1—H1···O2	C1—C2—C3—C4
IAM	1.142 (19)	1.270 (19)	2.4122 (7)	178.4 (17)	−2.1 (1)
Neutron	1.209 (3)	1.208 (3)	2.4163 (17)	176.0 (3)	−2.5 (2)
TAAM	1.218 (17)	1.194 (16)	2.4110 (3)	178.3 (14)	−2.0 (3)
MM_iso	1.177 (39)	1.239 (39)	2.4103 (5)	171.5 (37)	−2.0 (3)
MM_shade	1.166 (41)	1.253 (41)	2.4102 (5)	170.6 (37)	−2.0 (3)
HAR_iso	1.188 (17)	1.223 (17)	2.4106 (3)	178.4 (15)	−2.0 (1)
HAR_aniso	1.205 (18)	1.207 (18)	2.4113 (3)	177.3 (12)	−2.0 (1)
HAR_shade	1.192 (15)	1.219 (15)	2.4107 (3)	177.9 (14)	−2.0 (1)

HAR_iso, HAR_aniso and HAR_shade structures (Table 6) with similar precision (comparable standard uncertainties). The O1—H1—O2 angle is in turn a little different for MM_iso and MM_shade [171.5 (37)° and 170.6 (37)°, respectively] with lower precision and slightly different positions of O1 and O2 atoms in the hydrogen maleate ring. The IAM geometry, although similar to both MM geometries, is characterized by a more linear intramolecular hydrogen bond with the O1—H1—O2 angle equal to 178.4 (17)°.

The distance between O1 and O2 is very similar and precisely determined for each of the presented models, which enables a direct comparison of the O1—H1 and O2—H1 distances. Fig. 6 displays the difference between the O1—H1 and O2—H1 bond lengths for all the models together with the (averaged) standard uncertainties on the distances as error bars. The IAM refinement clearly falls behind all the other models, returning the most asymmetric geometry of the intramolecular hydrogen bond with O1—H1/O2—H1 distances of 1.142 (19)/1.370 (19) Å. The remaining methods yield a more symmetric geometry of the O1—H1···O2 interaction, particularly if standard uncertainties are considered. The values obtained for all three HAR refinement strategies are similar, but they can still be ordered by the difference between the O1—H1 and O2—H1 bond lengths. The hydrogen bond in HAR_aniso is highly symmetric [1.205 (18)/1.207 (18) Å], the other two structures exhibit a slight asymmetry [HAR_shade 1.192 (15)/1.219 (15) and HAR_iso 1.188 (17)/1.223 (17) Å]. For all the HAR refinements the precision of the determination of the bond lengths is high and the standard uncertainties similar. The TAAM structure is also characterized by a slightly asymmetric hydrogen bond [1.218 (17)/1.194 (16) Å] with a standard uncertainty comparable to HAR; however, H1 is shifted in the opposite direction than in the case of all the other methods. The parameters of the intramolecular hydrogen bond are very similar for both free multipole refinements leading to more asymmetric structures [MM_iso 1.177 (39)/1.239 (39) Å and MM_aniso 1.166 (41)/1.253 (41) Å] with standard uncertainties twice as high as those for the HAR and TAAM.

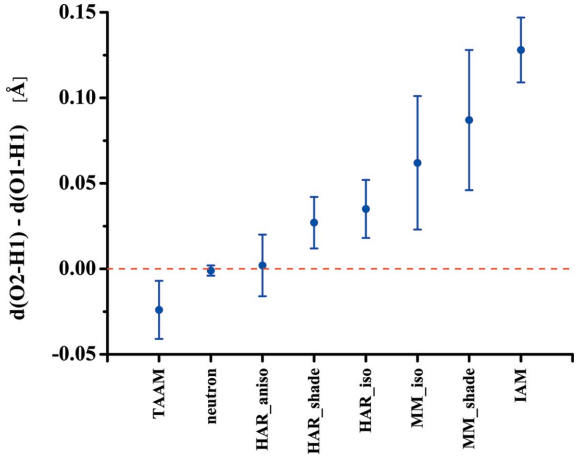

Figure 6
Difference between O2—H1 and O1—H1 distances for various methods of refinement with the averaged standard uncertainties for the O1/2—H1 distances marked on the plot.

This analysis implies that the anisotropic HAR refinement (HAR_aniso) gives a final geometry of the intramolecular hydrogen bond in best agreement with the neutron experiment. Taking into consideration the tilted shapes of the ellipsoids for many hydrogen atoms in this structure, it can be concluded that even some problems encountered during the refinement of hydrogen ADPs do not bias the geometry refinement performed according to the Hirshfeld procedure. The reason is probably that the diffraction pattern is determined by interference terms between oxygen- and hydrogen-atom form factors, which is a sensitive function of distance between the atoms. Even though hydrogen ADPs are not obtained well, the bond lengths are likely to be estimated correctly (compare discussion on hydrogen-atom ADP statistics in §3.1.1). The conclusion arising from the comparison of O1—H1/O2—H2 bond lengths in HAR_iso, HAR_shade and HAR_aniso structures (see Table 6) is that the more the refinement of geometry and hydrogen ADPs influence each other, the closer are the parameters of the hydrogen bond to those estimated in the neutron measurement, as the models can be ordered from the least to the most symmetric: HAR_iso (isotropic H), HAR_shade (H ADPs from *SHADE2*) and HAR_aniso (H ADPs refined). The TAAM refinement allows derivation of bond lengths and of the O1—H1···O2 angle similar to HAR, with a comparable precision. However, it must be remembered that the shown TAAM selected from a total of 12 TAAMs is the one with the most symmetric hydrogen bond. The hydrogen bond obtained after free multipole refinement (MM_iso and MM_shade) is least symmetric and also least precisely described. For these models, the geometry of the atoms forming the bond differs from the other models as well, and resembles more the IAM refinement than the neutron structure.

Closer observation of the strongest intermolecular hydrogen bond O5—H5···O3 linking the carboxyl group of the amino-acid cation (O5—H5) and the carbonyl atom O3 belonging to the anion is instructive. This bond is only slightly longer than the hydrogen bond existing within the anion (see Table 5), but it has a considerably different nature, due to the lack of chemical symmetry and linking two separate molecules

instead of atoms within the same rigid structure. A comparative study of the O5—H5···O3 bond in various density models demonstrates further differences between the investigated methods and confirms those revealed by the analysis of the O1—H1···O2 bond.

The neutron-diffraction study quantifies the O5—H5/O3—H5 bond lengths at 1.475 (3)/1.053 (3) Å and a short O5···O3 distance of 2.5231 (15) Å (Table 5). The bond is also less linear than the intramolecular one with the O5—H5···O3 angle amounting to 173.3 (3)°. Analysing the bond parameters for different models listed in Table 7, one observes that the O5···O3 distance is quite similar in all cases. However, comparison of the O5—H5/O3—H5 bond lengths clearly shows that the IAM refinement does not lead to the correct description of this hydrogen bond [O5—H5/O3—H5 equals 0.842 (15)/1.683 (15) Å]. A remarkable improvement is observed after HAR refinement. The geometry of the hydrogen bond in the structures HAR_shade and HAR_iso is quite close to the neutron geometry and HAR_aniso diverges marginally more. The angle in O5—H5···O3 is also close to the neutron structure for all the HAR models.

Table 7
Geometry of the intermolecular hydrogen bond O5—H5···O3 obtained with various refinement methods.

For the structures TAAM, MM_iso and MM_aniso the outcomes of two different O5—H5 bond treatments are listed: constrained to the average neutron value (first numerical value) and unconstrained (second numerical value). Units of distances and angles: Å, °.

Model	O5—H5	H5···O3	O5···O3	O5—H5···O3
IAM	0.842 (15)	1.683 (15)	2.5214 (7)	174.2 (15)
Neutron	1.053 (3)	1.475 (3)	2.5231 (15)	173.3 (3)
TAAM	1.018/0.943 (15)	1.502/1.578 (15)	2.5196 (3)/2.5198 (3)	178.30 (11)/176.6 (13)
MM_iso	1.018/0.944 (54)	1.503/1.578 (54)	2.5207 (5)/2.5206 (5)	178.47 (5)/177.2 (14)
MM_shade	1.018/0.932 (52)	1.503/1.589 (52)	2.5207 (5)/2.5205 (5)	178.40 (10)/177.2 (14)
HAR_iso	1.025 (15)	1.499 (15)	2.5206 (3)	174.4 (11)
HAR_aniso	1.014 (17)	1.508 (17)	2.5207 (3)	176.4 (13)
HAR_shade	1.027 (13)	1.497 (13)	2.5205 (3)	174.1 (10)

The outcomes of the refinement strategies based on the multipole model are not unambiguously favourable. As expected, for the TAAM, MM_iso and MM_aniso structures the geometry of the O5—H5···O3 bond is only comparable to the neutron geometry if the O5—H5 bond length is constrained to an averaged distance obtained by neutron diffraction taken from the literature. If the coordinates of H5 are refined without any constraints, the O5—H5 distance becomes too short to be regarded as physically correct. The conclusion is therefore that HAR, based on X-ray measurements of L-phenylalaninium hydrogen maleate, yields reliable hydrogen positions in strong hydrogen bonds, which is affirmed by the comparison with the neutron geometry, whereas multipole-model-based refinement strategies require significant intervention when performing structure refinement.

4. Conclusions

This study of L-phenylalaninium hydrogen maleate compares three methods of X-ray diffraction structure refinement – free multipole modelling (MM), transferable aspherical atom modeling (TAAM) and Hirshfeld atom refinement (HAR) – in terms of their ability to properly model strong hydrogen bonds, atomic displacement parameters and the total electron density of the crystal. Although each specified method constitutes a significant improvement in comparison with the independent atom model (IAM), still none approaches neutron measurements as far as accuracy and precision of the results are concerned. Certain trends and differences between the investigated refinement strategies emerge.

Methods based on the multipole model (MM and TAAM) do not allow unconstrained refinement, as opposed to HAR. Symmetry constraints must be imposed on atomic multipoles and X—H distances have to be fixed at averaged values from neutron diffraction. Otherwise hydrogen-atom properties become unreliable or they cannot be refined at all, *e.g.* in the case of anisotropic displacement parameters of hydrogen atoms. In HAR, X—H distances can be freely refined and their values are close to those derived from the neutron-diffraction experiment. Moreover, HAR renders refinement of hydrogen ADPs possible, which is shown to be in agreement with results from neutron diffraction within two combined standard uncertainties. Nevertheless, visual inspection of the hydrogen ADPs indicates unreasonable shapes and orientations. This relates to an insufficient amount of data describing atomic displacements at the given resolution or problems with the newly introduced $Z' > 1$ treatment. Nevertheless, the bond lengths obtained through HAR are not biased, and are most comparable to the results from the reference neutron-diffraction study.

Different starting points of HAR converge to very similar geometry, in particular the structures HAR_iso and HAR_shade are very much alike. In contrast, various TAAMs yield different geometry of the intramolecular hydrogen bond – a comparison with neutron measurements is necessary to choose the best model. However, the quality and precision of the results of the chosen TAAM are similar to those of HAR_iso and HAR_shade.

Although HAR, TAAM and MM yield adequate density models appropriate for chemical analysis of the derived electron density, the analysis of residual- and deformation-density maps clearly shows that HAR performs better than the multipole-model-based methods (TAAM and MM) in describing the measured diffraction pattern. Interestingly, this means that a purely theoretical electron-density determination technique based on an associated experimental geometry using a flexible basis set (HAR) agrees better with the experimental data than an experimental electron-density determination technique that is restricted by the inflexibility of its radial functions (MM).

With respect to the two strong hydrogen bonds of interest in this study (O1—H1···O2 and O5—H5···O3), it is clear that

the IAM performs very poorly for their modelling and it requires methods employing aspherical structure factors to describe them adequately. Among those techniques, only HAR_aniso reproduces the symmetric hydrogen site in the strong intramolecular hydrogen bond O1—H1···O2 that was found by neutron diffraction. For the strong intermolecular hydrogen bond O5—H5···O3, the O5—H5 distance is clearly underestimated in the multipole-based techniques (MM, TAAM), but in good agreement with the value from neutron diffraction in all three HAR models.

In view of the above considerations, HAR emerges with clear advantages over the multipole-model-based methods. In particular, if neutron data cannot be obtained, Hirshfeld atom refinement is the method of choice to obtain reliable hydrogen-atom properties from X-ray diffraction data.

The synchrotron-radiation experiments were performed on the BL02B1 beamline of SPring-8 with the approval of the Japan Synchrotron Radiation Research Institute (JASRI) under proposal No. 2013B1056. The neutron-diffraction experiments were performed on the KOALA beamline of the OPAL reactor under the Bragg Institute proposal No. 2160. MW, PMD and KW acknowledge the Polish NCN MAESTRO grant, decision number DEC-2012/04/A/ST5/00609. SG thanks the Australian Research Council for funding within the Discovery Project Grant DP110105347. The computational part of this work was performed using the computer cluster at the Computing Center of the Faculty of Chemistry, University of Warsaw, and the Interdisciplinary Centre for Mathematical and Computational Modeling, University of Warsaw (within the computational grant G53-17).

References

Alagar, M., Krishnakumar, R. V. & Natarajan, S. (2001). *Acta Cryst.* E**57**, o968–o970.

Alagar, M., Subha Nandhini, M., Krishnakumar, R. V., Mostad, A. & Natarajan, S. (2003). *Acta Cryst.* E**59**, o209–o211.

Allen, F. H. & Bruno, I. J. (2010). *Acta Cryst.* B**66**, 380–386.

Allen, F. H., Watson, D. G., Brammer, L., Orpen, A. G. & Taylor, R. (2006). *International Tables for Crystallography*, Vol. C, 1st online ed., ch. 9.5, pp. 790–811. Chester: International Union of Crystallography.

Bach, R. D., Dmitrenko, O. & Glukhovtsev, M. N. (1997). *J. Am. Chem. Soc.* **123**, 1081–1086.

Bąk, J. M., Domagała, S., Hübschle, C., Jelsch, C., Dittrich, B. & Dominiak, P. M. (2011). *Acta Cryst.* A**67**, 141–153.

Becke, A. D. (1993). *J. Chem. Phys.* **98**, 5648–5652.

Bendeif, E. & Jelsch, C. (2007). *Acta Cryst.* C**63**, o361–o364.

Betteridge, P. W., Carruthers, J. R., Cooper, R. I., Prout, K. & Watkin, D. J. (2003). *J. Appl. Cryst.* **36**, 1487.

Bindzus, N., Straasø, T., Wahlberg, N., Becker, J., Bjerg, L., Lock, N., Dippel, A.-C. & Iversen, B. B. (2014). *Acta Cryst.* A**70**, 39–48.

Blessing, R. H. (1987). *Crystallogr. Rev.* **1**, 3–58.

Capelli, S. C., Bürgi, H.-B., Dittrich, B., Grabowsky, S. & Jayatilaka, D. (2014). *IUCrJ*, **1**, 361–379.

Chandler, G. S. & Spackman, M. A. (1978). *Acta Cryst.* A**34**, 341–343.

Chęcińska, L., Morgenroth, W., Paulmann, P., Jayatilaka, D. & Dittrich, B. (2013). *CrystEngComm*, **15**, 2084–2090.

Czugler, M. & Báthori, N. (2004). *CrystEngComm*, **6**, 494–503.

Dadda, N., Nassour, A., Guillot, B., Benali-Cherif, N. & Jelsch, C. (2012). *Acta Cryst.* A**68**, 452–463.

Dittrich, B., Hübschle, C. B., Messerschmidt, M., Kalinowski, R., Girnt, D. & Luger, P. (2005). *Acta Cryst.* A**61**, 314–320.

Dittrich, B., McKinnon, J. J. & Warren, J. E. (2008). *Acta Cryst.* B**64**, 750–759.

Dittrich, B., Sze, E., Holstein, J. J., Hübschle, C. B. & Jayatilaka, D. (2012). *Acta Cryst.* A**68**, 435–442.

Dittrich, B., Weber, M., Kalinowski, R., Grabowsky, S., Hübschle, C. B. & Luger, P. (2009). *Acta Cryst.* B**65**, 749–756.

Dominiak, P. M., Makal, A., Mallinson, P. R., Trzcinska, K., Eilmes, J., Grech, E., Chruszcz, M., Minor, W. & Woźniak, K. (2006). *Chem. Eur. J.* **12**, 1941–1949.

Dominiak, P. M., Volkov, A., Li, X., Messerschmidt, M. & Coppens, P. (2007). *J. Chem. Theory Comput.* **3**, 232–247.

Dunning, T. H. (1989). *J. Chem. Phys.* **90**, 1007–1023.

Edwards, A. J. (2011). *Aust. J. Chem.* **64**, 869–872.

Fischer, A., Tiana, D., Scherer, W., Batke, K., Eickerling, G., Svendsen, H., Bindzus, N. & Iversen, B. B. (2011). *J. Phys. Chem. A*, **115**, 13061–13071.

Flack, H. D. (1983). *Acta Cryst.* A**39**, 876–881.

Frisch, M. J. *et al.* (2009). *Gaussian09*, Revision A.1. Gaussian Inc., Wallingford, CT, USA.

Garcia-Viloca, M., Gonzales-Lafont, A. & Lluch, J. M. (1997). *J. Am. Chem. Soc.* **119**, 1081–1086.

Hansen, N. K. & Coppens, P. (1978). *Acta Cryst.* A**34**, 909–921.

Hickstein, D. D., Cole, J. M., Turner, M. J. & Jayatilaka, D. (2013). *J. Chem. Phys.* **139**, 064108.

Hirshfeld, F. L. (1976). *Acta Cryst.* A**32**, 239–244.

Hirshfeld, F. L. (1977). *Theor. Chim. Acta*, **44**, 129–138.

Hodošček, M. & Hadži, D. (1990). *J. Mol. Struct. (Theochem)*, **209**, 411.

Hohenberg, P. & Kohn, W. (1964). *Phys. Rev. B*, **136**, 864–871.

Hoser, A. A., Dominiak, P. M. & Woźniak, K. (2009). *Acta Cryst.* A**65**, 300–311.

Hsu, B. & Schlemper, E. O. (1980). *Acta Cryst.* B**36**, 3017–3023.

Hussain, M. S., Schlemper, E. O. & Fair, C. K. (1980). *Acta Cryst.* B**36**, 1104–1108.

James, M. N. G. & Matsushima, M. (1976). *Acta Cryst.* B**32**, 1708–1713.

Jayatilaka, D. & Dittrich, B. (2008). *Acta Cryst.* A**64**, 383–393.

Jayatilaka, D. & Grimwood, D. J. (2003). *Tonto: a Fortran-Based Object-Oriented System for Quantum Chemistry and Crystallography.* New York: Springer.

Jin, Z. M., Hu, M. L., Wang, K. W., Shen, L. & Li, M. C. (2003). *Acta Cryst.* E**59**, o1–o3.

Jin, Z. M., Pan, Y. J., Hu, M. L. & Zou, J. W. (2002). *J. Mol. Struct.* **609**, 83–87.

Koritsanszky, T., Volkov, A. & Coppens, P. (2002). *Acta Cryst.* A**58**, 464–472.

Larson, A. C. (1970). *Crystallographic Computing*, edited by F. R. Ahmed, S. R. Hall & C. P. Huber, pp. 291–294. Copenhagen: Munksgaard.

Lee, C., Yang, W. & Parr, R. (1988). *Phys. Rev. B*, **37**, 785–789.

Lusi, M. & Barbour, L. J. (2011). *Cryst. Growth Des.* **11**, 5515–5521.

Madsen, A. Ø. (2006). *J. Appl. Cryst.* **39**, 757–758.

Madsen, A. Ø. (2012). *Struct. Bond.* **146**, 21–52.

Madsen, A. Ø., Sørensen, H. O., Flensburg, C., Stewart, R. F. & Larsen, S. (2004). *Acta Cryst.* A**60**, 550–561.

Madsen, D., Flensburg, C. & Larsen, S. (1998). *J. Phys. Chem. A*, **102**, 2177–2188.

Madsen, D. & Larsen, S. (1998). *Acta Cryst.* C**54**, 1507–1511.

Mallinson, P. R., Smith, G. T., Wilson, C. C., Grech, E. & Woźniak, K. (2003). *J. Am. Chem. Soc.* **125**, 4259–4270.

Meindl, K. & Henn, J. (2008). *Acta Cryst.* A**64**, 404–418.

Morgenroth, W., Overgaard, J., Clausen, H. F., Svendsen, H., Jørgensen, M. R. V., Larsen, F. K. & Iversen, B. B. (2008). *J. Appl. Cryst.* **41**, 846–853.

Munshi, P., Madsen, A. Ø., Spackman, M. A., Larsen, S. & Destro, R. (2008). *Acta Cryst.* A**64**, 465–475.
Olovsson, G., Olovsson, I. & Lehmann, M. S. (1984). *Acta Cryst.* C**40**, 1521–1526.
Pichon-Pesme, V., Jelsch, C., Guillot, B. & Lecomte, C. (2004). *Acta Cryst.* A**60**, 204–208.
Piltz, R. (2011). *Acta Cryst.* A**67**, C155.
Rajagopal, K., Krishnakumar, R. V., Mostad, A. & Natarajan, S. (2001). *Acta Cryst.* E**57**, o751–o753.
Rigaku (2004). *RAPID-AUTO*. Rigaku Corporation, Tokyo, Japan.
Santacruz, L., Abonia, R., Cobo, J., Low, J. N. & Glidewell, C. (2007). *Acta Cryst.* C**63**, o585–o587.
Schwarzenbach, D., Abrahams, S. C., Flack, H. D., Prince, E. & Wilson, A. J. C. (1995). *Acta Cryst.* A**51**, 565–569.
Sheldrick, G. M. (2008). *Acta Cryst.* A**64**, 112–122.
Stewart, R. F., Bentley, J. J. & Goodman, B. (1975). *J. Chem. Phys.* **63**, 3786–3793.
Sugimoto, K., Ohsumi, H., Aoyagi, S., Nishibori, E., Moriyoshi, C., Kuroiwa, Y., Sawa, H. & Takata, M. (2010). *AIP Conf. Proc.* **1234**, 887–891.
Vanhouteghem, F., Lenstra, A. T. H. & Schweiss, P. (1987). *Acta Cryst.* B**43**, 523–528.
Volkov, A., Li, X., Koritzanszky, T. S. & Coppens, P. (2004). *J. Phys. Chem. A*, **108**, 4283–4300.
Volkov, A., Macchi, P., Farrugia, L. J., Gatti, C., Mallinson, P., Richter, T. & Koritsanszky, T. (2006). *XD2006 – A Computer Program Package for Multipole Refinement, Topological Analysis of Charge Densities and Evaluation of Intermolecular Energies from Experimental and Theoretical Structure Factors*.
Volkov, A., Messerschmidt, M. & Coppens, P. (2007). *Acta Cryst.* D**63**, 160–170.
Wilkinson, C., Khamis, H. W., Stansfield, R. F. D. & McIntyre, G. J. (1988). *J. Appl. Cryst.* **21**, 471–478.
Wilson, C. C., Thomas, L. H. & Morrison, C. A. (2003). *Chem. Phys. Lett.* **381**, 102–108.
Woźniak, K., Mallinson, P. R., Smith, G. T., Willson, C. C. & Grech, E. (2003). *J. Phys. Org. Chem.* **16**, 764–771.
Zarychta, B., Pichon-Pesme, V., Guillot, B., Lecomte, C. & Jelsch, C. (2007). *Acta Cryst.* A**63**, 108–125.
Zhurov, V. V. & Pinkerton, A. A. (2013). *Z. Anorg. Allg. Chem.* **639**, 1969–1978.
Zhurov, V. V., Zhurova, E. A., Stash, A. I. & Pinkerton, A. A. (2011). *Acta Cryst.* A**67**, 160–173.